Algal Research 9 (2015) 263–274

Contents lists available at ScienceDirect

Algal Research

journal homepage: www.elsevier.com/locate/algal

# Modelling of light and temperature influences on cyanobacterial growth and biohydrogen production

D. Zhang [a], P. Dechatiwongse [b], E.A. del Rio-Chanona [a], G.C. Maitland [b], K. Hellgardt [b], V.S. Vassiliadis [a,*]

[a] Department of Chemical Engineering and Biotechnology, University of Cambridge, Pembroke Street, Cambridge CB2 3RA, UK
[b] Department of Chemical Engineering, Imperial College London, South Kensington Campus, London SW7 2AZ, UK

ARTICLE INFO

*Article history:*
Received 20 November 2014
Received in revised form 22 February 2015
Accepted 22 March 2015
Available online 3 April 2015

*Keywords:*
Biohydrogen production
Cyanobacteria
Dynamic simulation
Light intensity
Light attenuation
Temperature

ABSTRACT

Dynamic simulation is a valuable tool to assist the scale-up and transition of biofuel production from laboratory scale to potential industrial implementation. In the present study two dynamic models are constructed, based on the Aiba equation, the improved Lambert–Beer's law and the Arrhenius equation. The aims are to simulate the effects of incident light intensity, light attenuation and temperature upon the photo-autotrophic growth and the hydrogen production of the nitrogen-fixing cyanobacterium *Cyanothece* sp. ATCC 51142. The results are based on experimental data derived from an experimental setup using two different geometries of laboratory scale photobioreactors: tubular and flat-plate. All of the model parameters are determined by an advanced parameter estimation methodology and subsequently verified by sensitivity analysis. The optimal temperature and light intensity facilitating biohydrogen production in the absence of light attenuation have been determined computationally to be 34 °C and 247 μmol $m^{-2}$ $s^{-1}$, respectively, whereas for cyanobacterial biomass production they are 37 °C and 261 μmol $m^{-2}$ $s^{-1}$, respectively. Biomass concentration higher than 0.8 g $L^{-1}$ is also demonstrated to significantly enhance the light attenuation effect, which in turn inducing photolimitation phenomena. At a higher biomass concentration (3.5 g $L^{-1}$), cyanobacteria are unable to activate photosynthesis to maintain their lives in a photo-autotrophic growth culture, and biohydrogen production is significantly inhibited due to the severe light attenuation.



## 1. Introduction

Carbon dioxide, $CO_2$, is the major source of environmental concern for causing global warming and it is mainly released by burning carbon-based energy resources such as petrol, coal and natural gas [21]. Meanwhile, it is accepted that it is unsustainable to continuously rely on limited and nonrenewable conventional fuels [8]. To reduce the production of $CO_2$ and fulfil the increasing demand for energy, novel sustainable and environmentally friendly energy sources are being sought. Biofuels such as biodiesel, biohydrogen, and ethanol are expected to provide new opportunities to replace conventional fossil fuels and diversify sustainable energy sources [22]. Biofuels are produced by microalgae mainly through photosynthesis, whereby $CO_2$ is fixed into carbohydrates such as lipids, starch and sugars via different metabolic pathways. Lipids are usually used to generate biodiesel, while starch and sugars are always converted to ethanol, hydrogen and other biofuels [30]. Conventional diesel and gasoline can be replaced by biodiesel and bioethanol, respectively. Biohydrogen is mainly used within fuel cells and as a transport fuel due to its high heat of combustion [9,22].

Biohydrogen is considered to be the most promising bio-energy carrier as there is no release of $CO_2$ during its combustion [17]. The $CO_2$ fixed during microalgal photosynthesis is mainly used to compose the cell structure of microalgae. Hence, theoretically, biohydrogen generated in bioprocesses can be considered to be carbon-neutral. Another attractive advantage of generating biohydrogen from microalgae is that microalgae have been utilised as healthy food because of their high nutritional value. For instance, microalgae have been served as food in China and Mexico from ancient times [10]. Therefore, the $CO_2$ derived microalgal biomass can be concurrently sold as a by-product of the biohydrogen generation process, which could make the process more economical [13].

Recent research found that *Cyanothece* sp. ATCC 51142 (*Cyanothece* 51142), a type of nitrogen-fixing unicellular cyanobacterium, offers remarkably high rates of $H_2$ production, which have never been observed before in any other hydrogen-producing strain [5]. Although *Cyanothece* 51142 contains both hydrogenase and nitrogenase for biohydrogen production, previous research has demonstrated that the nitrogen-fixing process regulated by nitrogenase is predominant reaction, and hydrogen production rates employing this metabolic process are

* Corresponding author.
*E-mail address:* vsv20@cam.ac.uk (V.S. Vassiliadis).

http://dx.doi.org/10.1016/j.algal.2015.03.015

**Nomenclature**

| | |
|---|---|
| $\alpha_g$ | Bubble volume fraction |
| $\tau_c$ | Light extinction coefficient by cell absorption |
| $\mu_{max}$ | maximum specific growth rate |
| $A_c$ | Pre-exponential factor for cyanobacterial growth |
| $A_d$ | Pre-exponential factor for cyanobacterial decay |
| $d_b$ | Average bubble diameter |
| $E_a$ | Activation energy for cyanobacterial growth |
| $E_{a;H2}$ | Activation energy for hydrogen production |
| $E_b$ | Inactivation energy for cyanobacterial decay |
| $H_2$ | Hydrogen production |
| I | Light intensity cells experience |
| $I_0$ | Incident light intensity |
| $k_i$ | Light photoinhibition coefficient |
| $k_{i;H2}$ | Nitrogenase light photoinhibition coefficient |
| $K_N$ | Nitrate half-velocity coefficient |
| ks | Light saturation coefficient |
| $k_{s;H2}$ | Nitrogenase light saturation coefficient |
| N | Nitrate concentration |
| $T_a$ | Reference temperature for cyanobacterial growth |
| $T_{a;H2}$ | Reference temperature for enzyme activation |
| $T_b$ | Reference temperature for cyanobacterial decay |
| $T_{b;H2}$ | Reference temperature for enzyme inactivation |
| X | Biomass concentration |
| z | Thickness of photobioreactor |

significantly higher than those in photosynthesis processes stimulated by hydrogenase [24]. Additionally, compositional analyses of *Cyanothece* 51142 show that this strain contains high levels of protein (60%) and carbohydrate (29%) with low levels of fat (less than 1%) [28], which indicates its high potential of being refined to health food. As a result, this species is being extensively studied at present.

However, challenges of biohydrogen production from *Cyanothece* 5 1142 still greatly restrict its further development, and the evolution of biofuel production from laboratory scale to industrial scale has to be implemented [27]. High biomass density cultivation is seen as the major challenge at the current stage [8]. In a lab scale photobioreactor (PBR), biomass concentration usually reaches densities of 1 g $L^{-1}$–3 g $L^{-1}$ where the culture is highly dense [3,12]. Even when excess nutrients are present in the culture medium, cyanobacteria are not able to grow because of the serious light attenuation observed in PBRs. Although recent research [3] demonstrated that cyanobacteria can be cultivated up to 12 g $L^{-1}$ in a laboratory scale, the incident light intensity provided in that case was relatively high (457 μmol $m^{-2}$ $s^{-1}$) which would add cost for the necessary lighting.

While a number of studies have been conducted to analyse the influence of light intensity and temperature on *Cyanothece* 51142 growth and biohydrogen production [3,14,16,24], much less research has focused on the aspects of cell growth and hydrogen production with regard to light attenuation, which always exists and is difficult to be eliminated and analysed in experiments. Furthermore, it is also very time consuming to seek the optimal temperature and light intensity for cell growth and biohydrogen production rate purely by experiments. As a result, the current research aims to explore the effect of light intensity, light attenuation and temperature on the *Cyanothece* 51142 growth rate and biohydrogen production rate by dynamic simulation.

## 2. Experimental setup and data selection

### 2.1. Experimental setup

Input data for our simulation were obtained from experimental studies using two different geometries of photobioreactor: tubular and flat-plate. To investigate the cyanobacterial growth kinetics, a tubular flow Biostat PBR 2S was our reactor choice [12], whereas an Imperial College flat-plate PBR [32] was utilised for the study of $H_2$ production. The reason behind our PBR selection is based on the main features of each PBR. Specifically, the tubular PBR enables an automated and consistent control of cultivating conditions and was thus used for the study of growth kinetics. In the case of $H_2$ production kinetics study, our customised flat-plate PBR was employed instead, due to its gas-tight design as well as ability to in-situ measure $H_2$. During the growth study [12], *Cyanothece* 51142 culture was cultivated in an artificial sea water (ASP2) with supplement of 1.5 g $L^{-1}$ $NaNO_3$ and 10% volume $CO_2$ volume $air^{-1}$ under continuous illumination of cool-white fluorescent using seven light regimes (23, 46, 92, 138, 207, 275 and 320 μmol $m^{-2}$ $s^{-1}$) and constant temperature at 35 °C. In the case of temperature effects, a fixed light intensity of 92 μmol $m^{-2}$ $s^{-1}$ was employed and our investigated regimes were 25, 30, 32, 35, 37 and 40 °C.

For $H_2$ productivity study [14], a non-heating illumination provided by a panel of cool-white 5000 K light-emitting diodes (LED) was used. As an anaerobic environment is necessary for the onset of cyanobacterial $H_2$ production, glycerol was chosen to replace $CO_2$ as carbon source. In the presence of glycerol, photosynthetic activities of *Cyanothece* 51142 are inhibited, whereas the respiratory activity becomes enhanced [4,15]. The culture of *Cyanothece* 51142 was initially subjected into the ASP2 medium with a supplement of 50 mM glycerol. As soon as $H_2$ production was observed, the switch in operating conditions was made. The temperature regimes were 20, 25, 30, 35, 40, 47 and 55 °C and the light intensity regimes were 46, 92, 138, 229, 320 μmol $m^{-2}$ $s^{-1}$. The dry biomass concentration of the *Cyanothece* 51142 culture was derived from its spectrophotometrically measured chlorophyll concentration, using a previously determined correlation in our work [12]. The hydrogen production rate of the cyanobacterial culture was in situ measurement using a membrane-inlet mass spectrometry (MIMS) system [32]. Details of the experimental setup and the execution of these experiments can be found in [12,14].

### 2.2. Data selection

In order to truly simulate light intensity and temperature influences on cyanobacterial growth, it is vital to ensure that nutrients are in excess and not the growth-limiting factors. During our experimental studies, sufficiency of the carbon source was ensured by a continuous provision of $CO_2$, whereas the nitrogen source, nitrate, always ran out at the end of experiments (except during the runs with incident light intensity $I_0 = 23$ μmol $m^{-2}$ $s^{-1}$ and $I_0 = 46$ μmol $m^{-2}$ $s^{-1}$) [12]. Therefore, the data for our simulation were selected during the nitrate-sufficient period where nitrate concentration was higher than 500 mg $L^{-1}$.

A similar principle was applied to simulate the environmental effects on hydrogen production rate. Our previous research showed that the gas is mainly produced during the cyanobacterial second growth and the decay phases [15]. However, during the latter phase, the activity of nitrogenase was not only affected by light intensity and temperature, but also significantly affected by acidity (low pH environment) of the culture phase [15]. As a result, the data were selected during the cyanobacterial second growth phase and the early decay phase, where the pH was still in an appropriated range (between 6 and 8) and cyanobacterial decay rate was not significant.

## 3. Construction of kinetic models and calculation theory

### 3.1. Introduction of dynamic models

Generally, cyanobacterial growth rate is strongly influenced by various factors such as nutrient concentration, temperature and light intensity. Temperature usually affects the activity of biochemical enzymes, involved in the cellular reproduction process, whereas light intensity determines the energy cells can absorb for their maintenance and growth. Elements including sulphur, carbon, phosphorus and nitrogen are necessary for cyanobacteria to compose their biomass structure [12].

The kinetics of cyanobacterial growth is usually described by the Monod model and the Droop Model which only consider the effect of nutrient concentration [34,36], because other parameters e.g. temperature and light intensity are always kept constant during experiments. In the Monod model, as shown in Eq. (1), the maximum specific growth rate $\mu_{max}$ is treated as a constant, but in reality it is a function of light intensity and temperature. When nutrients are in excess, the growth rate is independent of nutrient concentration and the term of $\frac{N}{K_N+N}$ approaches 1. To obtain high biomass concentration, it is vital to maintain the optimal environmental conditions, which can maintain the growth rate to its maximum value. Realistically, as the rate of biomass accumulation is the balance between reproduction and decay terms, Eq. (1) is thus revised to Eq. (2).

The second term on the right hand side of Eq. (2) represents the respiration rate of cyanobacteria, which can be derived from the Logistic model [12] (detailed derivation is presented in Appendix A). The current work assumes that cyanobacterial respiration rate is only a function of temperature, as previous research usually measures cell respiration rate from the experiments under a completely dark environment [23].

$$\frac{dX}{dt} = \mu_{max} \cdot \frac{N}{K_N + N} \cdot X \tag{1}$$

$$\frac{dX}{dt} = \alpha \cdot k(I) \cdot k(T) \cdot X - \alpha_d \cdot k_d(T) \cdot X^2 \tag{2}$$

where $N$ denotes nutrient concentration, $\mu_{max}$ denotes maximum specific growth rate, $k(I)$ denotes effects of light intensity on cell growth, $k(T)$ denotes effects of temperature on cell growth, $k_d(T)$ denotes effects of temperature on cell respiration, and $\alpha$ and $\alpha_d$ denote the effect of nutrients on cell growth and cell respiration rate, respectively.

Similar to growth, $H_2$ production kinetics of cyanobacteria is also influenced by temperature and light intensity, as its production is directed by an enzymatic and energy-dependent nitrogen-fixing reaction [16]. As previous research [15] demonstrated that hydrogen production rate is proportional to biomass concentration, the model used for hydrogen production simulation can be expressed by Eq. (3). Since cyanobacteria stop growing after the depletion of nitrate and nitrogenase activity starts to recover once the culture is nitrate-free, hydrogen is mainly produced during the stationary and decay phases where biomass growth rate is zero. Therefore in the current study, it is assumed that the hydrogen production rate is a function of biomass concentration but independent on biomass growth rate.

$$\frac{dX}{dt} = \alpha_{H2} \cdot h(I) \cdot h(T) \cdot X \tag{3}$$

where $h(I)$ denotes effects of light intensity on hydrogen production rate, $h(T)$ denotes effects of temperature on hydrogen production rate, and $\alpha_{H2}$ denotes effects of nutrients on hydrogen production rate.

### 3.2. Simulation of light intensity influences

Light is always the primary limiting factor necessary for cell growth and $H_2$ production of green algal and cyanobacterial cultures. The Aiba model, shown in Eq. (4), is usually employed to simulate the effect of light intensity on cyanobacterial growth rate [1]. The Aiba model is capable of modelling the photolimitation regime under low light intensity circumstances, the photosaturation regime under optimal light intensity circumstance, and the photoinhibition regime under intense light intensity conditions[38]. Similarly, the model can also be applied to describe the photo-dependence of the hydrogen production rate, as shown in Eq. (5).

$$k(I) = \frac{I}{I + k_s + \frac{I^2}{k_i}} \tag{4}$$

$$h(I) = \frac{I}{I + k_{s,H2} + \frac{I^2}{k_{i,H2}}} \tag{5}$$

where $k_s$ is the light saturation coefficient for cell growth, μmol $m^{-2}$ $s^{-1}$, $k_i$ is the light prohibition coefficient for cell growth, μmol $m^{-2}$ $s^{-1}$, $k_{s,H2}$ is the light saturation coefficient for hydrogen production, μmol $m^{-2}$ $s^{-1}$, and $k_{i,H2}$ is the light prohibition coefficient for hydrogen production, μmol $m^{-2}$ $s^{-1}$.

### 3.3. Simulation of temperature influences

Arrhenius' equation is generally demonstrated to effectively simulate thermal effects on bacterial growth rate [2,7,33]. Eq. (6) shows the typical Arrhenius' equation, while for the convenience of parameter estimation in the current study, Eq. (6) is transformed to Eq. (7). As $\alpha$ (specific growth rate, $hr^{-1}$) and $\alpha_d$ (specific decay rate, L $g^{-1}\cdot hr^{-1}$) are converted to $T_a$ and $T_b$, the exponential terms in Arrhenius' equation will contain their units. Overall, $k(T)$ and $k_d(T)$ have the units of ($hr^{-1}$) and (L $g^{-1}\cdot hr^{-1}$), respectively.

$$\frac{dX}{dt} = \alpha \cdot k(I) \cdot A_c \cdot \exp\left[-\frac{E_a}{RT}\right] \cdot X - \alpha_d \cdot A_d \cdot \exp\left[-\frac{E_b}{RT}\right] \cdot X^2 \tag{6}$$

$$\frac{dX}{dt} = k(I) \cdot \exp\left[-\left(\frac{E_a}{RT} - \frac{E_a}{RT_a}\right)\right] \cdot X - \exp\left[-\left(\frac{E_b}{RT} - \frac{E_b}{RT_b}\right)\right] \cdot X^2 \tag{7}$$

where $A_c$ and $A_d$ are pre-exponential factors. $E_a$ is activation energy and $E_b$ is inactivation energy.

Similarly, temperature effects on the hydrogen production rate can be described by Eq. (8a) as gas production is directed by nitrogenase. Another revised Arrhenius' equation, Eq. (8b), is also found to be capable of well representing both the positive and negative impacts of temperature on enzyme activity, and has been applied in the recent work [6]. Therefore, it is subsequently selected to compare with Eq. (8a). The units of $h(T)$ in both equations are mL $g^{-1}$.

$$h(T) = \exp\left[-\left(\frac{E_{a,H2}}{RT} - \frac{E_{a,H2}}{RT_{a,H2}}\right)\right] - \exp\left[-\left(\frac{E_{b,H2}}{RT} - \frac{E_{b,H2}}{RT_{b,H2}}\right)\right] \tag{8a}$$

$$h(T) = \frac{\exp\left[-\left(\frac{E_{a,H2}}{RT} - \frac{E_{a,H2}}{RT_{a,H2}}\right)\right]}{1 + \exp\left[-\left(\frac{E_{b,H2}}{RT} - \frac{E_{b,H2}}{RT_{b,H2}}\right)\right]} \tag{8b}$$

### 3.4. Modelling of light attenuation influence

During our experiments it was possible to only measure incident light intensity, which is not the same as the local radiance experienced by cells. In fact, significant light attenuation of our flat plate PBR and Sartorius tubular PBR was observed at high biomass concentration, and is shown in Fig. 1. Eq. (4) is modified by including the light attenuation term in order to improve the precision of our model.

Within the culture liquid phase, local light intensity in a PBR is attenuated by three factors: (i) microbial absorption, (ii) bubble reflection and (iii) water reflection.

Earlier research [11,29] has demonstrated that in the liquid–gas multiphase system light is mainly scattered by bubbles and absorbed by microalgae. In high biomass cultivation, microbial absorption is always the primary factor for light attenuation (Fig. 1(b)) [29]; while in low biomass cultivation, bubble reflection becomes the predominant factor leading light attenuation (Fig. 1(a)) [37]. The recent research [37] has proposed an equation (Eq. (9)) to calculate local light intensities in a PBR by including both factors. Since the extinction coefficient of *Cyanothece* 51142 has not been measured before, the current work will also estimate this value based on the experimental data.

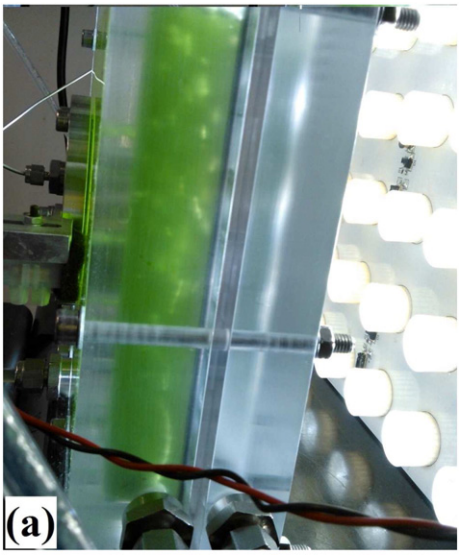


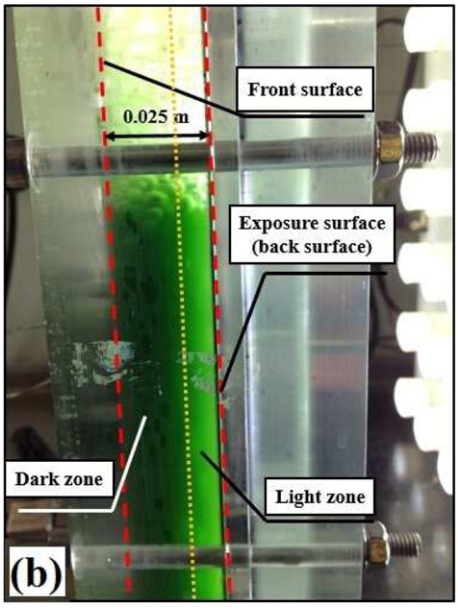


**Fig. 1.** Light attenuation in the 1 L flat-plate photobioreactor. (a) Biomass concentration is 0.08 g $L^{-1}$; (b) biomass concentration is 1.88 g $L^{-1}$.

$$I = I_0 \cdot \exp\left[-\left(\frac{3\cdot\alpha_g}{d_b}+\tau_c\cdot X\right)\cdot z\right] \tag{9}$$

where $\alpha_g$ is bubble volume fraction, $d_b$ is average bubble diameter, m, $\tau_c$ is extinction coefficient of biomass, $m^2\ g^{-1}$ (dry weight) which has not been measured in the current research, $X$ is biomass concentration, g (dry weight) $L^{-1}$, and $z$ is the thickness of the PBR, m. $\alpha_g$ (0.0067) has been calculated and $d_b$ has been measured in our previous study [37].

### 3.5. Simulation of photobioreactor

Within a well-mixed PBR, a uniform distribution of temperature is always achieved in the liquid culture. However light attenuation is strongly dependent on the thickness of the PBR, as well as the changes in local light intensity along the direction of light transmission (shown in Eqs. (10a) and (10b)). Therefore the kinetic model includes both spatial dimension (light transmission direction) and time dimension.

$$k(I) = \frac{I(t,z)}{I(t,z)+k_s+\dfrac{I^2(t,z)}{k_i}} \tag{10a}$$

$$I(t,z) = I_0(t,z)\cdot\exp\left[-\left(\frac{3\cdot\alpha_g}{d_b}+\tau_c\cdot X(t,z)\right)\cdot z\right] \tag{10b}$$

For the convenience of parameter estimation, the average cyanonbacterial growth rate is used and shown in Eqs. (11a) and (11b) to render the model one-dimensional.

$$\frac{dX}{dt} = \overline{k}(I)\cdot k(T)\cdot X(t) - k_d(T)\cdot X^2(t) \tag{11a}$$

$$\begin{aligned}\overline{k} = (I) &= \frac{1}{L}\cdot\int_0^L k(I)dz \\ &= \frac{1}{L}\cdot\int_0^L \frac{I_0\cdot\exp\left[-\left(\frac{3\cdot\alpha_g}{d_b}+\tau_c\cdot X\right)\cdot z\right]}{I_0\cdot\exp\left[-\left(\frac{3\cdot\alpha_g}{d_b}+\tau_c\cdot X\right)\cdot z\right]+k_s+\frac{\left(I_0\cdot\exp\left[-\left(\frac{3\cdot a_g}{d_b}+\tau_c\cdot X\right)\cdot z\right]\right)}{k_i}}dz\end{aligned} \tag{11b}$$

However, the reduced kinetic models are still two-dimensional and the parameters are difficult to estimate. To simplify the parameter estimation process, Eq. (11b) was solved by an approximate numerical integration method named the Trapezoidal rule due to its wide application [31]. To ensure the accuracy of the parameter estimation process, a 10-step approximation formula was applied initially (shown in Appendix A), and was verified later (detailed verification is shown in Section 4.2). Similarly, when simulating the influence of incident light intensity on hydrogen production rate, the average hydrogen production rate $\overline{h}(I)$ is also calculated by this method.

Finally, Eqs. (12a) and (12b) are used to simulate the influence of incident light intensity and temperature on cyanobacterial growth and hydrogen production, respectively.

$$\frac{dX}{dt} = \overline{k}(I)\cdot\exp\left[-\left(\frac{E_a}{RT}-\frac{E_a}{RT_a}\right)\right]\cdot X - \exp\left[-\left(\frac{E_b}{RT}-\frac{E_b}{RT_b}\right)\right]\cdot X^2 \tag{12a}$$

$$\frac{dH_2}{dt} = \overline{h}(I)\cdot h(T)\cdot X \tag{12b}$$

### 3.6. Parameter estimation methodology

A major factor in dynamic modelling is the accurate estimation of model parameters. To estimate the parameters for the current

models, the following nonlinear least-squares optimisation problem is formulated:

$$\min_p \Phi(p) = \sum_{i=1}^{N} (\hat{y}_i - y(t_i,p))^T \Lambda_i (\hat{y}_i - y(t_i,p)) \tag{13a}$$

subject to:

$$\frac{dx}{dt} = f(x(t),p) \tag{13b}$$

$$x_{lb} \le x \le x_{ub} \tag{13c}$$

$$p_{lb} \le p \le p_{ub} \tag{13d}$$

$$t = t_0,\ x = x_0 \tag{13e}$$

where $x_{lb}$, $x_{ub}$, $p_{lb}$, and $p_{ub}$ are lower and upper bounds for the state variables and parameters respectively.

The objective function is a general weighted least-squares formula, where Λ is the weighting matrix, as here measurement variances come in. Given the nonlinearity and stiffness of the dynamic optimisation least-squares model in Eqs. (13a)–(13e), orthogonal collocation over finite elements in time is used throughout this paper due to its high accuracy [36]. As hydrogen production kinetics and biomass growth kinetics are decoupled, in the current study two independent parameter estimation problems are solved to determine parameter values in each model.

The implementation in this work was carried out in a Python environment. Pyomo [19], an open source tool package for modelling optimisation applications in Python, was used as the interface and the specific optimisation solver used was IPOPT [35] (linked as a library in Pyomo). Results were obtained on an Intel Core i5, 4 GB RAM, 2.53 GHz laptop computer.

## 4. Results and discussion

### 4.1. Results of parameter estimation

By performing parameter estimation, all of the constants in our kinetic models were successfully determined and are presented in Table 1. It can be seen from the table that our evaluated parameters are highly comparable with previously reported data, thereby indicating the high level of reliability in our results. However, the value of $k_i$ obtained in the current research is much lower than the literature reported values. Theoretically, the maximum of $k(I)$ in Eq. (4) is $\frac{1}{1+2\cdot\left(\frac{k_s}{k_i}\right)^{0.5}}$ only when $I = \sqrt{k_s \cdot k_i}$, and photoinhibition will be observed if $I$ is higher than the optimum (detailed derivation is shown in the Appendix A). As most of previous published work assumes a uniform distribution of illumination inside the PBRs, the light intensity cell experience ($I$) is thus the same with the incident light intensity ($I_0$). However, this assumption is generally unacceptable as the uniform distribution of illumination is quite difficult to ensure, and in reality two different zones, light zone and dark zone, were observed receptively in the front and dark part of the reactor in this research (Fig. 1b). Therefore $I$ is always much lower than $I_0$. Because of this severe light extinction, even when the incident light intensity is high, photoinhibition may only appear in a small area close to the light source of PBRs, while the major part is controlled by photolimitation. Hence, when increasing $I_0$ the final biomass concentration will still be enhanced. As a result, the value of $\sqrt{k_s \cdot k_i}$ is greatly overestimated due to the replacement of $I$ by $I_0$. In particular, because of the experimentally undetectable effects of photoinhibition, the overestimation of $\sqrt{k_s \cdot k_i}$ will result in a significantly overestimated $k_i$.

In terms of data fitting, Figs. 2 and 3 show the data fitting of *Cyanothece* 51142 growth profile at different incident light intensity and temperature regimes, respectively. From the two figures, it is seen that the current kinetic models can accurately describe both light and temperature dependence of cyanobacterial growth from 46 to 320 μmol $m^{-2}$ $s^{-1}$ in terms of light intensity, and from 25 °C to 40 °C in terms of temperature. The maximum fitting error is also found not to exceed 10%. The reason of the inability of the models at 23 μmol $m^{-2}$ $s^{-1}$ based on our assumption is that photosynthesis may not be able to conduct at such a low radiance. A slight overestimation was found when simulating the cyanobacterial growth rate at light intensity set to 320 μmol $m^{-2}$ $s^{-1}$. In this experiment, as the biomass growth rate is high due to the high incident light intensity, the consumption rates of both nitrate and $CO_2$ are also elevated. Therefore, cell growth may also be limited by nutrient concentration and thus the overestimation observed with the current model arises.

Similarly, Table 2 and Fig. 4 show the data fitting results in terms of the $H_2$ production under different incident light intensity and temperature conditions, respectively. These comparisons indicate that our model is valid at light intensity higher than 92 μmol $m^{-2}$ $s^{-1}$, below which a large deviation (15.5% when incident light intensity is 46 μmol $m^{-2}$ $s^{-1}$) is observed, and for a temperature range from 20 °C to 55 °C. This deviation is possibly due to the low average light intensity in the PBR, which is not capable of stimulating the activity of nitrogenase since this reaction is very energy consuming [20].

Although both Eqs. (8b) and (8a) appear to perfectly fit our experimental data between 20 and 40 °C, Eq. (8b) fails to describe the very sharp thermal inhibition above 47 °C (320 K), where nitrogenase is found totally inactivated and not able to generate hydrogen in the

**Table 1**
Parameters estimated in the current research.

| Parameter and units | Simulation result | Literature result | Ref. |
|---|---|---|---|
| $k_s$ [μmol $m^{-2}$ $s^{-1}$] | 165 | [70,250] | [6,39,40] |
| $k_i$ [μmol $m^{-2}$ $s^{-1}$] | 457 | [2760,53370] | |
| $k_{s,H2}$ [μmol $m^{-2}$ $s^{-1}$] | 138 | [70,250] | |
| $k_{i,H2}$ [μmol $m^{-2}$ $s^{-1}$] | 457 | [610,53370] | |
| $\tau_c$ [$m^2$ $g^{-1}$] | 0.126 | [0.067,0.225] | |
| $E_a$ [kJ $mol^{-1}$] | 55.4 | [37.5, 122.5] | [6,7,41,42] |
| $E_b$ [kJ $mol^{-1}$] | 389.9 | [127.5, 654] | |
| $T_a$ [K] | 327.9 | [301.4, 355.8] | |
| $T_b$ [K] | 317.8 | [308.21, 337.3] | |
| $E_{a,H2}$ in Eq. (8) [kJ $mol^{-1}$] | 76.28 | [37.5, 122.5] | |
| $E_{a,H2}$ in Eq. (9) [kJ $mol^{-1}$] | 63.79 | [37.5, 122.5] | |
| $E_{b,H2}$ in Eq. (8) [kJ $mol^{-1}$] | 127.4 | [127.5, 654] | |
| $E_{b,H2}$ in Eq. (9) [kJ $mol^{-1}$] | 326.6 | [127.5, 654] | |
| $T_{a,H2}$ in Eq. (8) [K] | 273.6 | [277.8, 292.3] | |
| $T_{a,H2}$ in Eq. (9) [K] | 272.4 | [277.8, 292.3] | |
| $T_{b,H2}$ in Eq. (8) [K] | 288.8 | [279.8, 337.3] | |
| $T_{b,H2}$ in Eq. (9) [K] | 308.8 | [279.8, 337.3] | |

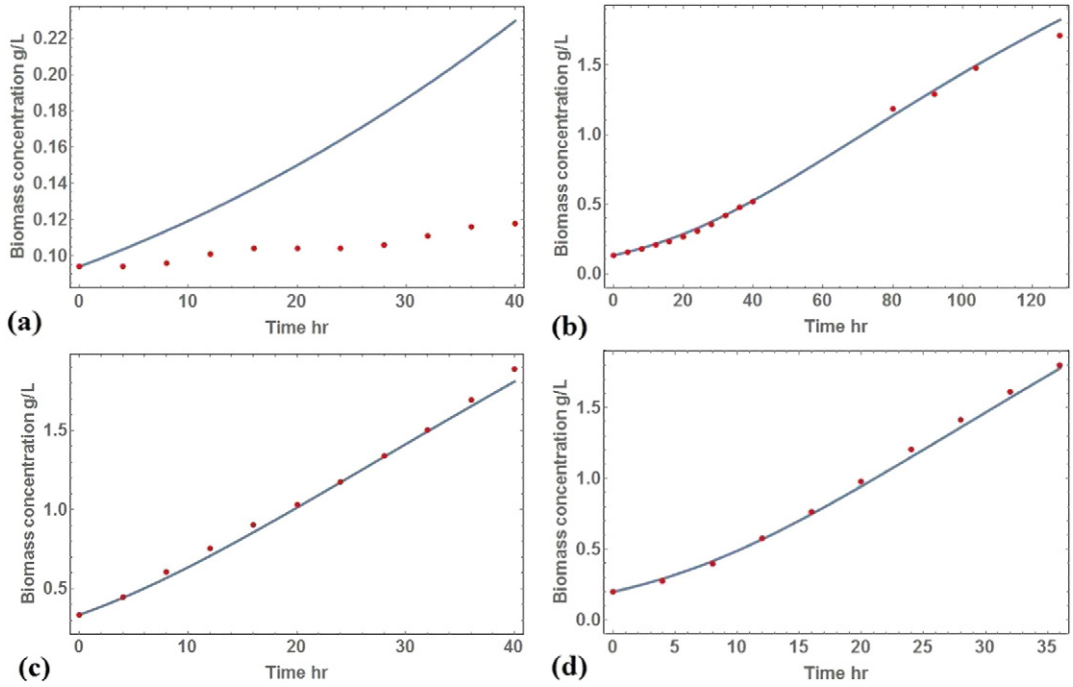


**Fig. 2.** Comparison of simulation and experimental results of light intensity effects on cyanobacterial growth. The culture temperature is 35 °C. (a), Incident light intensity: 23 μmol $m^{-2}$ $s^{-1}$; (b), incident light intensity: 46 μmol $m^{-2}$ $s^{-1}$; (c), incident light intensity: 138 μmol $m^{-2}$ $s^{-1}$; (d), incident light intensity: 207 μmol $m^{-2}$ $s^{-1}$.

present experiment work. Therefore, only Eq. (8a) is chosen for further analysis.

### 4.2. Verification of numerical integration method

To ensure the reliability of parameters evaluated in the current work, the accuracy of the approximate numerical integration method has to be verified. In the present research, the NDSolve subroutine in Wolfram Mathematica® 10.0 is selected to calculate the true result of $k(I)$ and $h(I)$. The NDSolve subroutine is a highly accurate package to solve differential equations. The package includes a variety of methods to solve different types of differential equations, and can automatically use an adaptive procedure to determine the size of integration steps and integration order.

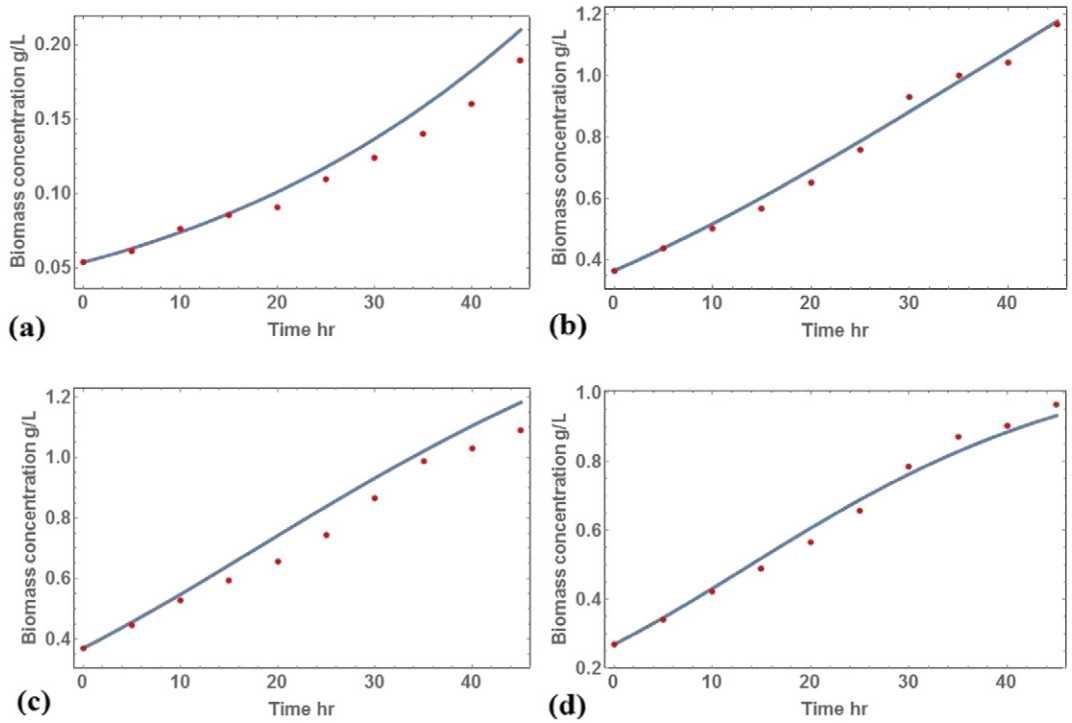


**Fig. 3.** Comparison of simulation and experimental results of temperature effects on cyanobacterial growth. The incident light intensity is 92 μmol $m^{-2}$ $s^{-1}$. (a), temperature: 25 °C; (b), temperature: 32 °C; (c), temperature: 35 °C; (d), temperature: 37 °C.

**Table 2**
Maximum deviation of simulation results of light intensity effects on hydrogen production rate. The culture temperature is 35 °C.

| Incident light intensity | Simulation result | Experimental result | Deviation |
|---|---|---|---|
| 46 μmol $m^{-2}$ $s^{-1}$ | 1.148 mL $g^{-1}$ $h^{-1}$ | 1.358 mL $g^{-1}$ $h^{-1}$ | 15.5% |
| 92 μmol $m^{-2}$ $s^{-1}$ | 2.480 mL $g^{-1}$ $h^{-1}$ | 2.696 mL $g^{-1}$ $h^{-1}$ | −9.3% |
| 138 μmol $m^{-2}$ $s^{-1}$ | 3.259 mL $g^{-1}$ $h^{-1}$ | 3.320 mL $g^{-1}$ $h^{-1}$ | 1.8% |
| 229 μmol $m^{-2}$ $s^{-1}$ | 3.320 mL $g^{-1}$ $h^{-1}$ | 3.320 mL $g^{-1}$ $h^{-1}$ | 0.0% |
| 320 μmol $m^{-2}$ $s^{-1}$ | 3.721 mL $g^{-1}$ $h^{-1}$ | 3.729 mL $g^{-1}$ $h^{-1}$ | 0.2% |

Because $k(I)$ and $h(I)$ are functions of biomass concentration, it is essential to compare the deviation of true and approximate results at different biomass concentrations. The highest biomass concentration in the entire range of experimental data is 2.15 g $L^{-1}$, and in most cases the biomass concentration ranges from 0.8 g $L^{-1}$ to 1.5 g $L^{-1}$. Table 3 lists the deviation between $k(I)$ and $\bar{k}(I)$ when the biomass concentration ranges from 0.2 g $L^{-1}$, the initial concentration in the current experiments, to 12.0 g $L^{-1}$, the highest concentration found in current publications [3].

From Table 3, it was found that the 5-step method can give an accurate approximation up to a concentration of 3 g $L^{-1}$ (deviation of 12.1%), beyond which the 10-step method should be employed instead (deviation of 5.17%). As our recorded maximum concentration is 2.15 g $L^{-1}$, the latter method is verified as an effective approach for numerical approximation. However the 10-step method only validates up to 6 g $L^{-1}$. For higher concentrations, the 20-step method has to be used until the biomass concentration is 12 g $L^{-1}$. If the present numerical integration method is applied for modelling a high cell density culture, it is then important to change the 10-step method to the 20-step method.

### 4.3. Verification of parameter estimation methodology

An efficient parameter estimation methodology should guarantee that the optimum of most parameters can be found. The objective function used in the current estimation process is defined as Eq. (13a). When the value of parameters in a model diverges from its optimum, the value of the least squares error objective function will increase. Therefore by exploring the change of objective function in terms of small changes (±5%) in the parameter values, the quality of the parameter estimation methodology can be verified [26]. In specific, the weight factors appearing in Eq. (13a) are chosen in this section to be equal to 1. This is because the aim here is to explore the change of the objective function due to the change of parameter values, rather than fitting the parameter values in the current model.

Fig. 5 shows the contour plots of Eq. (13a) as functions of different combinations of parameters including $E_{a,H2}$, $T_{a,H2}$, $E_{b,H2}$, $T_{b,H2}$, $k_s$, $k_i$ and $\tau_c$. The value of the objective function is the same when the combination of two parameters is chosen from the same contour. In Fig. 5, the value

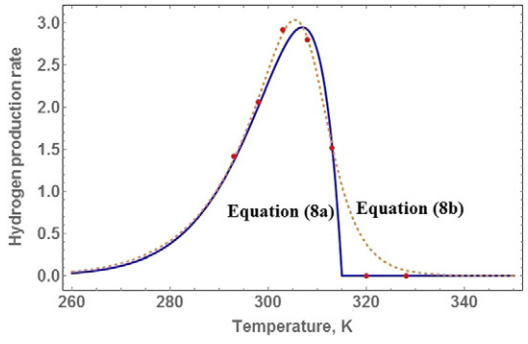


**Fig. 4.** Comparison of simulation and experimental results of temperature effects on maximum hydrogen production rate (mL $L^{-1}$ $h^{-1}$). The incident light intensity is 92 μmol $m^{-2}$ $s^{-1}$. Solid line: simulation result based on Eq. (8a); dashed line: simulation result based on Eq. (8b); circle point: experimental result.

**Table 3**
Accuracy of numerical integration method. For the 5-step integration method the step length is 0.005 m; for the 10-step integration method the step length is 0.0025 m; for the 20-step method the step length is 0.00125 m. The incident light intensity is 138 μmol $m^{-2}$ $s^{-1}$.

| Biomass | 5-Step | | 10-Step | | 20-Step | | NDSolve |
|---|---|---|---|---|---|---|---|
| | Result | Deviation | Result | Deviation | Result | Deviation | |
| 0.2 g·$L^{-1}$ | 0.326 | 0.31% | 0.326 | 0.31% | 0.326 | 0.31% | 0.327 |
| 0.5 g·$L^{-1}$ | 0.249 | 2.05% | 0.249 | 2.05% | 0.249 | 2.05% | 0.244 |
| 1.0 g·$L^{-1}$ | 0.164 | 4.46% | 0.163 | 3.82% | 0.162 | 3.18% | 0.157 |
| 1.5 g·$L^{-1}$ | 0.118 | 5.36% | 0.116 | 3.57% | 0.115 | 2.68% | 0.112 |
| 2.0 g·$L^{-1}$ | 0.092 | 8.24% | 0.089 | 4.71% | 0.088 | 3.53% | 0.085 |
| 3.0 g·$L^{-1}$ | 0.065 | 12.1% | 0.061 | 5.17% | 0.060 | 3.45% | 0.058 |
| 4.0 g·$L^{-1}$ | 0.053 | 23.3% | 0.047 | 9.30% | 0.045 | 4.65% | 0.043 |
| 5.0 g·$L^{-1}$ | 0.047 | 34.3% | 0.038 | 8.57% | 0.037 | 5.71% | 0.035 |
| 6.0 g·$L^{-1}$ | 0.044 | 51.7% | 0.033 | 13.8% | 0.031 | 6.90% | 0.029 |
| 8.0 g·$L^{-1}$ | 0.041 | 86.4% | 0.027 | 22.7% | 0.024 | 9.09% | 0.022 |
| 10.0 g·$L^{-1}$ | 0.040 | 122% | 0.023 | 27.8% | 0.019 | 5.56% | 0.018 |
| 12.0 g·$L^{-1}$ | 0.040 | 167% | 0.022 | 46.7% | 0.017 | 13.3% | 0.015 |

of contours in the middle zone is much lower than that in the outer zone. It can be seen that all of the parameters estimated by the current methodology are optimal, which indicates the high accuracy of current methodology.

### 4.4. Sensitivity analysis

Sensitivity analysis is a common tool to explore the change of model output (usually the yield of process products) with respect to the change of parameters in kinetic models [18,36]. To optimise the model output, it is essential to know the relationship between the parameters and the output. As parameters in the current models have their specific physical meanings, sensitivity analysis can direct the development of new mutants and process operating conditions by manipulating the most sensitive parameters to enhance the yield of products in fermentation processes.

The definition of normalised sensitivity is shown in Eq. (14) [25]. Sensitivity indicates the proportional change of model output ($y$) due to the proportional change of parameters ($x$). A positive sensitivity indicates that an increase of $x$ results in an increase of $y$, while a negative sensitivity suggests that increasing $x$ will lead to a decrease of $y$. In particular, in the current models the output either refers to biomass concentration or to hydrogen yield. Fig. 6 shows the sensitivity of the two outputs with respect to each parameter.

$$S_{y/x} = \frac{dy}{dx} \cdot \frac{x}{y} \tag{14}$$

where $y$ is the model output and $x$ is the parameter in kinetic models.

The sensitivity of $H_2$ yield with respect to each model parameter is calculated during the brief cyanobacterial stationary phase, between the second growth and the decay phases where the activity of nitrogenase remains significant and cell death rate is not high [15]. As shown in Fig. 7 [15], constant biomass concentration and nitrogenase-mediated $H_2$ production rate were observed, subsequently this brief phase can be considered as steady-state. During this steady-state condition, the sensitivity of gas production rate is independent of time.

Fig. 6 illustrates the sensitivity of both cyanobacterial biomass concentration and $H_2$ yield with respect to each parameter. It can be clearly seen that both outputs are predominantly influenced by activation energy ($E_a$ and $E_{a,H2}$), activation reference temperature ($T_a$ and $T_{a,H2}$) and inactivation reference temperature ($T_b$ and $T_{b,H2}$).

In particular, $T_a$ and $T_{a,H2}$ are found to dramatically suppress both outputs, and their effect is about 10-fold higher than that of other parameters. For example, a 1% increase of $T_a$ and $T_{a,H2}$ can lead to a 20% decrease of maximum biomass concentration and to a 40% decrease of

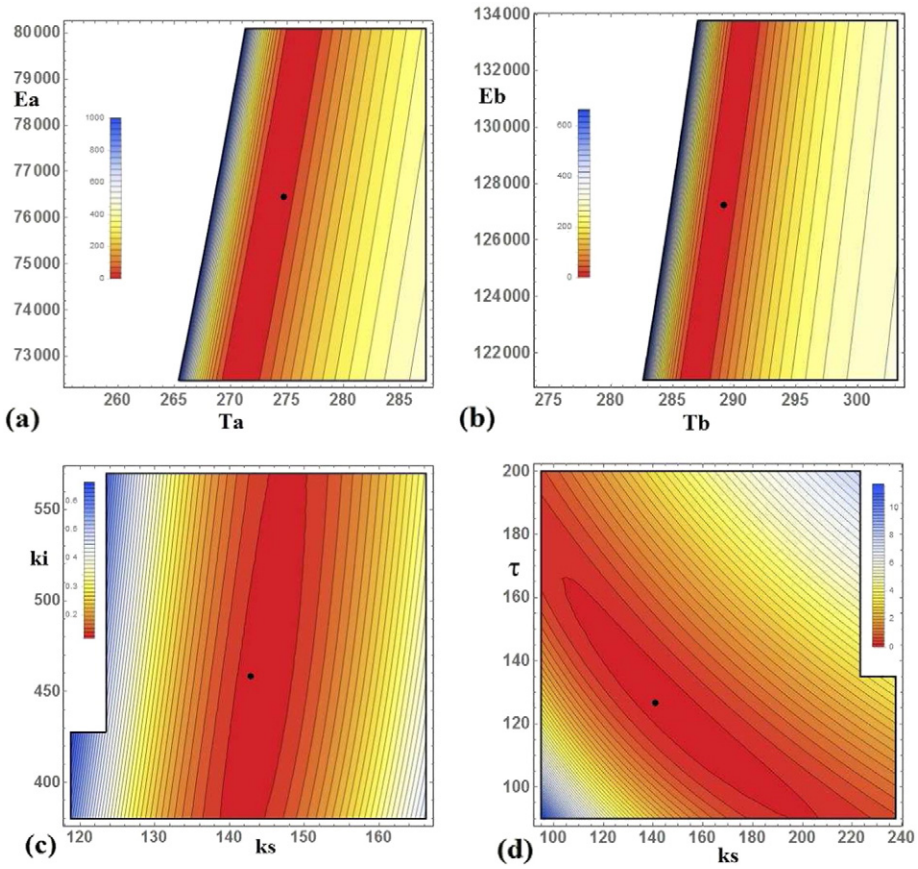


**Fig. 5.** Contour plots of the objective function as a function of different combinations of parameters. (a), $E_{a,H2}$ (J/mol) and $T_{a,H2}$ (K); (b), $E_{b,H2}$ and $T_{b,H2}$; (c), $k_s$ and $k_i$; (d), $k_s$ and $\tau_c$. The black point in each figure represents the value of each parameter.

total hydrogen yield. The reason why both biomass concentration and hydrogen yield are very sensitive to $T_a$ and $T_{a,H2}$ can be explained in two aspects. On one hand, these parameters combine the effects of both nutrient concentrations and temperature (the definition of $T_a$ and $T_{a,H2}$ can be found in the previous section); on the other hand which is more important, the exponential functionality with respect to temperature makes any chemical reaction very sensitive to temperature compared to any other parameters, which enters either linearly or through some power law relationship. However, the effect of the inactivation energy ($E_b$ and $E_{b,H2}$) for both outputs of interest is not important. Parameters involved in both the Aiba and the light attenuation equations show a much smaller impact on both biomass concentration and hydrogen yield.

### 4.5. Effects of light intensity on cyanobacterial growth and hydrogen production

Sensitivity analysis was applied to study the effects of incident light intensity, $I_0$, and local light intensity, $I$, on both cyanobacterial biomass growth and hydrogen production rates, as defined by Eqs. (15a) and (15b). The local light intensity represents the actual light radiance experienced by cyanobacteria. Attention should be paid on the definition of cyanobacterial growth and $H_2$ production rate in different cases. As the incident light intensity is expressed in Eq. (15a), both rates refer to the average rates inside the PBR. In contrast, these rates are considered as local rates in Eq. (15b), since the local light intensity is present.

$$S_{y/I_0} = \frac{dy}{dI_0} \cdot \frac{I_0}{y} \tag{15a}$$

$$S_{y/I} = \frac{dy}{dI} \cdot \frac{I}{y} \tag{15b}$$

where y is the either cyanobacterial growth or $H_2$ production rate.

Sensitivities of $H_2$ production rate (mL $g^{-1}$ $h^{-1}$) and cells growth rate ($h^{-1}$) with regard to $I_0$, and $I$ are shown in Fig. 8. From Fig. 8, it is found that the optimum actual light intensity (local light intensity) for hydrogen production and cyanobacterial growth is 247 μmol $m^{-2}$ $s^{-1}$ and 261 μmol $m^{-2}$ $s^{-1}$, respectively. When the cyanobacterial culture is exposed at a local light intensity higher than the optimum, the photoinhibition phenomenon begins to take place as the sensitivity of cell growth and hydrogen production rates becomes negative. However, an incident light intensity lower than 731 μmol $m^{-2}$ $s^{-1}$ is always found facilitating the average rate of both physiological processes. This striking difference is caused predominantly by light attenuation in the PBR. Since the effects of light attenuation on cell growth and hydrogen production are very similar, the current study focuses on cyanobacterial growth rate as an example for detailed explanations.

### 4.6. Effects of light attenuation on cell growth and hydrogen production

Fig. 9 shows the local cyanobacterial growth rate from the exposure surface (back surface) to the front surface at different incident light intensities and biomass concentrations. The distance from the back surface (exposure surface) to the front surface of the flat plate PBR is 0.025 m (detailed description is shown in Fig. 1). Three clearly different profiles of local light intensity and cyanobacterial growth rate can be observed when the biomass concentration increases from 0.08 g $L^{-1}$ to 3.5 g $L^{-1}$.

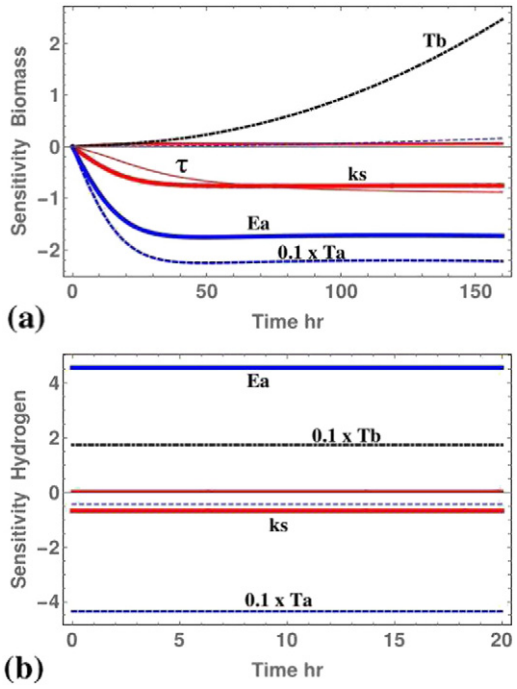


**Fig. 6.** Sensitivity analysis of the current models. (a), Sensitivity of biomass concentration with respect to each parameter ($E_a$, $T_a$, $E_b$, $T_b$, $k_s$, $k_i$, $\tau_c$) when incident light intensity is 138 μmol $m^{-2}$ $s^{-1}$ and temperature is 30 °C; (b), sensitivity of hydrogen yield with respect to each parameter ($E_{a,H2}$, $T_{a,H2}$, $E_{b,H2}$, $T_{b,H2}$, $k_{s,H2}$, $k_{i,H2}$, $\tau_c$) when incident light intensity is 138 μmol $m^{-2}$ $s^{-1}$, temperature is 30 °C and cyanobacteria are the brief stationary phase. "0.1×" means the sensitivity of model output with respect to the specific parameter is 10-fold of that shown in the figure.

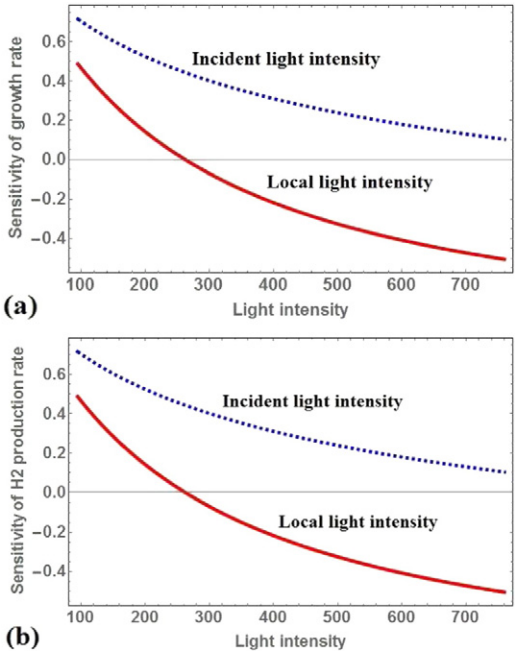


**Fig. 8.** Sensitivity of cell growth and hydrogen production rates w.r.t. light intensity. (a), Sensitivity of cell growth rate with respect to light intensity; (b), sensitivity of hydrogen production rate with respect to light intensity. Dashed line: incident light intensity (biomass concentration is 0.8 g $L^{-1}$), solid line: local light intensity.

Light attenuation is mainly contributed by bubble scattering and cyanobacterial absorption. Based on the current model, it is found that during the initial stage of experiments when the culture is dilute (0.08 g $L^{-1}$), both light scatter and cell absorption are important for light attenuation, as the value of the term representing bubble reflection ($\frac{3\cdot\alpha_g}{d_b}$) in Eq. (9) is the same with that ($\tau_c \cdot X$) denoting cell absorption. Even at such a dilute biomass concentration and low bubble volume fraction, light attenuation in the reactor is not negligible as the local light intensity on the front surface is reduced by 40% (Fig. 9(d)). However because of the high incident light intensity and low biomass concentration, photoinhibition dominates the entire part of the PBR when the incident light intensity is 457 μmol $m^{-2}$ $s^{-1}$ and 686 μmol $m^{-2}$ $s^{-1}$ (Fig. 9(a)), as local cyanobacterial growth rate increases with the decreasing local light intensity from the exposure surface to the front surface.

However, when biomass concentration increases to 0.8 g/L (Fig. 9(b)), light attenuation in the PBR becomes much more remarkable and local light intensity in the front part of PBR is lower than 20% of the incident light intensity (Fig. 9(d)). Cell absorption becomes the primary factor for light attenuation compared to bubble reflection, as the value of this term in Eq. (9) is 10 times higher than the bubble scatter term. Because of the severe cyanobacterial absorption, photoinhibition only dominates the back part of the PBR (0.00–0.005 m from the back surface (exposure surface) of the reactor) while photolimitation controls the front part of the PBR (0.010–0.025 m) when the incident light intensity is 457 μmol $m^{-2}$ $s^{-1}$ and 686 μmol $m^{-2}$ $s^{-1}$ (Fig. 9(b)). Thus, cyanobacteria cannot grow effectively due to the remarkably non-uniform distribution of local light intensity.

Nevertheless, if biomass concentration is much more dense, for example 3.5 g $L^{-1}$ as found in our experimental work [12], local light intensity is less than 23 μmol $m^{-2}$ $s^{-1}$ at the cross-section only 0.01 m beyond the light-incoming surface along the direction of light transmission, even if the incident light intensity is 686 μmol $m^{-2}$ $s^{-1}$. Due to such a notable light attenuation in the PBR, cell growth rate is even lower than the cell respiration rate in half of the PBR regardless of the incident light intensity, as the net cell growth rate is negative (shown in Fig. 9(c)). Therefore, cyanobacteria cannot survive under photo-autotrophic growth conditions in the dark part of the PBR. Hydrogen is not produced as the local light intensity is not high enough to rapidly replenish the energy consumed in the hydrogen production metabolic pathway (nitrogen-fixing process).

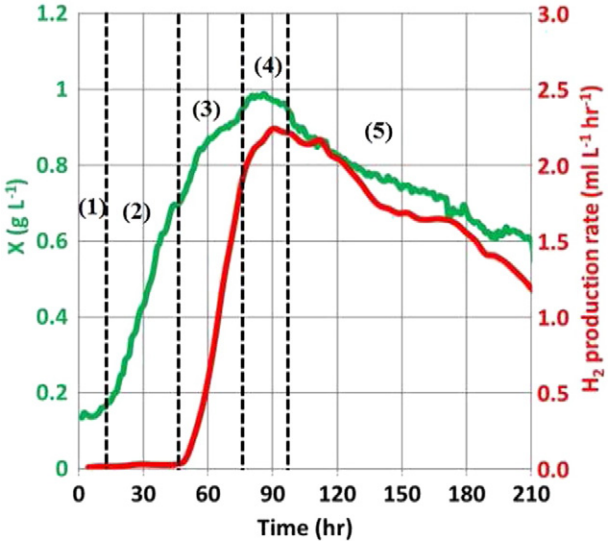


**Fig. 7.** Different growth phases of cyanobacteria [15]. (1), Lag phase; (2), first growth phase; (3), second growth phase; (4), stationary phase; (5), decay phase.

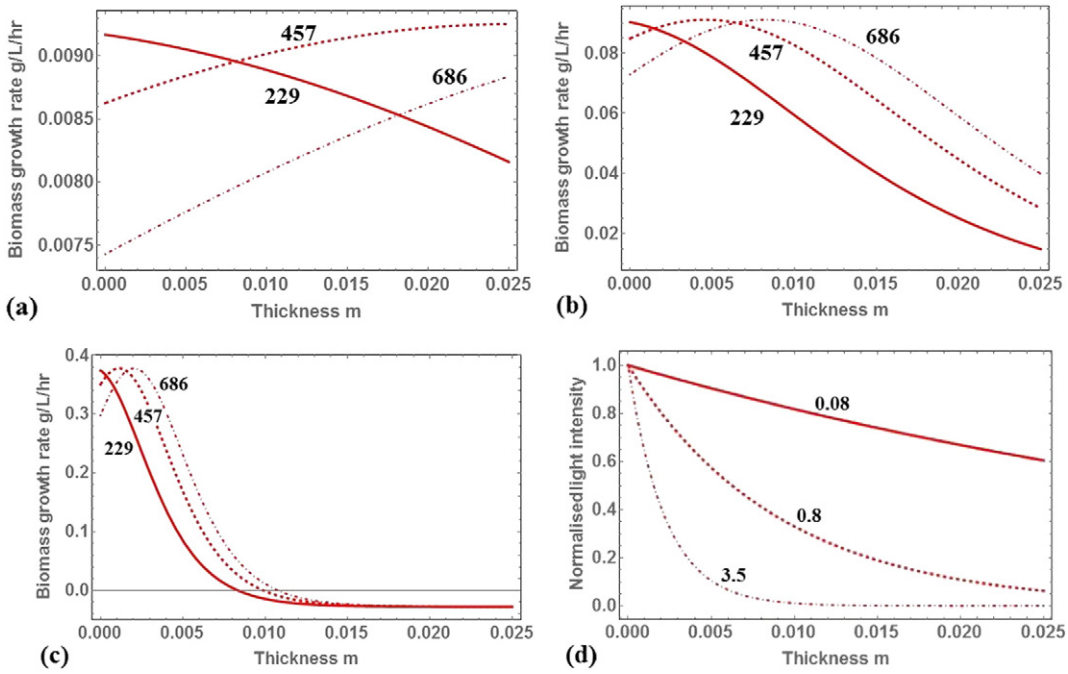


**Fig. 9.** Local cyanobacterial growth rate at different incident light intensities and biomass concentrations. (a), Local cyanobacterial growth rate when biomass concentration is 0.08 g $L^{-1}$, and incident light intensity is 229 μmol $m^{-2}$ $s^{-1}$, 457 μmol $m^{-2}$ $s^{-1}$ and 686 μmol $m^{-2}$ $s^{-1}$; (b), local cyanobacterial growth rate when biomass concentration is 0.8 g/L, and incident light intensity is 229 μmol $m^{-2}$ $s^{-1}$, 457 μmol $m^{-2}$ $s^{-1}$ and 686 μmol $m^{-2}$ $s^{-1}$; (c), local cyanobacterial growth rate when biomass concentration is 3.5 g $L^{-1}$, and incident light intensity is 229 μmol $m^{-2}$ $s^{-1}$, 457 μmol $m^{-2}$ $s^{-1}$ and 686 μmol $m^{-2}$ $s^{-1}$; (d), normalised local light intensity when biomass concentration is 0.08 g $L^{-1}$, 0.8 g $L^{-1}$ and 3.5 g $L^{-1}$. 0.00 in x-axis represents the back surface of the reactor and 0.025 represents the front surface.

### *4.7. Effects of temperature on cyanobacterial growth and hydrogen production*

The same concept of sensitivity analysis is also applied to study temperature effects. The definition of sensitivity with regard to temperature is shown by Eq. (16).

$$S_{y/T} = \frac{dy}{dT} \cdot \frac{T}{y} \tag{16}$$

where $y$ is the cyanobacterial growth rate or hydrogen production rate.

Fig. 10 shows that optimum temperatures for hydrogen production and cyanobacterial growth are 34 °C and 37 °C, respectively. It is also found that the rates for both processes are very sensitive to the culture temperature. When the culture temperature is lower than the optimum, a 1% increase in temperature can significantly enhance both cell growth rate and hydrogen production rate by 20%. However once the temperature exceeds the optimal value, the same temperature increase can cause remarkable damage on the photosynthetic apparatus of the cyanobacterium and subsequently lead to a sharp decrease of both rates (23% for the growth rate and 50% for the hydrogen production rate) [14].

## 5. Conclusion

In our present study, dynamic models based on the Aiba equation, the improved Lambert–Beer's law, and the improved Arrhenius equation were constructed to explore the effects of light and temperature on cyanobacterial photo-autotrophic growth and hydrogen production of the nitrogen-fixing cyanobacterium *Cyanothece* 51142. Parameter estimation methodologies and sensitivity analyses were conducted to guarantee the accuracy of the proposed models. It is found that both cyanobacterial growth and hydrogen production rates are very susceptible to the parameters of the Arrhenius equation, which means that the effects of temperature are more significant compared to those of illumination. The optimal light intensity and temperature for biomass and hydrogen productions were determined. Finally, it is concluded that when the biomass concentration is higher than 0.8 g $L^{-1}$, light attenuation inside the PBR becomes the major limiting factor. Under highly dense culture conditions (>3.5 g $L^{-1}$), local light intensity could become less than

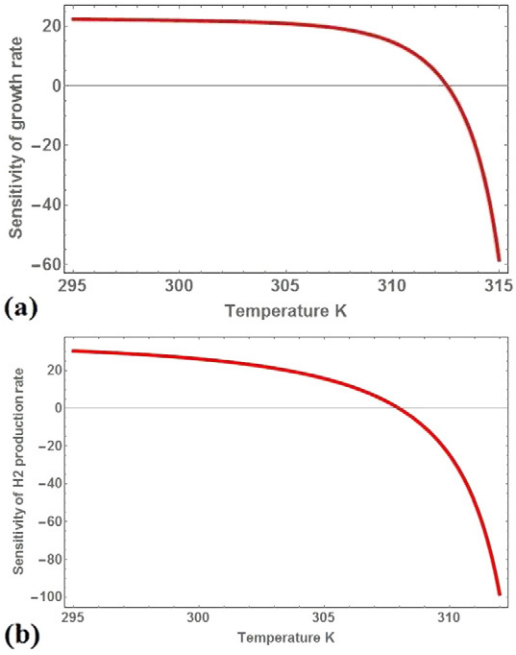


**Fig. 10.** Sensitivity of hydrogen production and cell growth rates w.r.t. temperature. (a), Sensitivity of cell growth rate with respect to temperature when biomass concentration is 0.2 g $L^{-1}$; (b), sensitivity of hydrogen production rate with respect to temperature.

23 μmol $m^{-2}$ $s^{-1}$ within 0.01 m from the exposure surface, even when an intense incident light intensity of 686 μmol $m^{-2}$ $s^{-1}$ is applied. Under such circumstances, cyanobacterial cells in the most part within the PBR are unable to harness light energy for either cell growth or hydrogen production.

In terms of the future work, the current models will be applied to analyse the effects of PBR configuration on both cell growth and hydrogen production, and to predict the production of hydrogen and biomass in different scale reactors. In addition, flash effects should also be included in future work, since cyanobacteria are not necessary to experience light continuously. After receiving photons, cyanobacterial photosystems will switch to the excited state and illumination is not essential for photosynthesis. By optimising the culture mixing rate so that cells can always move to the light zone after their photosystems change back to the ground state, the apparent photoactive volume of the system will have the potential to be enhanced.

## 6. During the conduction of this article

Author Dongda Zhang's contributions included the construction of dynamic models, the simulation of photobioreactor, the optimisation of operating conditions and the drafting of the article.Author Pongsathorn Dechatiwongse's contributions included conception and design of the experiments, collection and assembly of data, as well as critical revision of the article for important intellectual content.Author Ehecatl Antonio del Rio-Chanona's contributions include the development of novel parameter estimation methodology for model construction, the verification of model accuracy, and the drafting of the article.Author Geoffrey C. Maitland and Klaus Hellgardt involved the design of experiments, and provided funding and critical revision of the article for important intellectual content as well as gave the final approval of the article.Author Vassilios S. Vassiliadis involved the development and verification of the dynamic simulation solver and critical revision of the article for important intellectual content as well as gave the final approval of the article. He also had critical overview of the direction of theproject and the development strategy of this paper.

## Acknowledgement

The author D. Zhang gratefully acknowledges the support from his family. The author P. Dechatiwongse is supported by a scholarship from the Royal Thai Government, Thailand, and his project, Solar Hydrogen Project, was funded by the UK Engineering and Physical Sciences Research Council (EPSRC), project reference EP/F00270X/1. Author E. A. del Rio-Chanona is funded by CONACyT scholarship No. 522530 from the Secretariat of Public Education and the Mexican government. The authors wish to thank Mr. Fabio Fiorelli for his invaluable advice and support during the preparation of this work.

## Appendix A

### A.1. Derivation of photo-autotrophic growth equation

$$X(t) = \frac{X_{max}}{1 + \exp[-\mu \cdot (t - t_0)]}$$

$$\frac{dX(t)}{dt} = \frac{X_{max} \cdot \mu \cdot \exp[-\mu \cdot (t - t_0)]}{(1 + \exp[-\mu \cdot (t - t_0)])^2}$$

$$= \frac{X_{max} \cdot \mu \cdot (\exp[-\mu \cdot (t - t_0)] + 1) - X_{max} \cdot \mu}{(1 + \exp[-\mu \cdot (t - t_0)])^2}$$

$$= \frac{X_{max} \cdot \mu}{1 + \exp[-\mu \cdot (t - t_0)]} - \frac{X_{max}^2}{(1 + \exp[-\mu \cdot (t - t_0)])^2} \cdot \frac{\mu}{X_{max}}$$

$$= \mu \cdot X(t) - \frac{\mu}{X_{max}} \cdot X^2(t)$$

$$= \mu \cdot X(t) - \mu_d \cdot X^2(t)$$

### A.2. Derivation of maximum k(I)

$$k(I) = \frac{I}{I + k_s + \frac{I^2}{k_i}}$$

$$\frac{dk(I)}{dI} = \frac{k_s - \frac{I^2}{k_i}}{\left(I + k_s + \frac{I^2}{k_i}\right)^2}$$

When $k(I)$ researches its maximum value, the first derivation of $k(I)$ on $I$ should be 0. Therefore:

$$I_{opt} = \sqrt{k_s \cdot k_i}.$$

For hydrogen production the optimal light intensity is 247 μmol $m^{-2}$ $s^{-1}$, and for cyanobacterial biomass production the optimal light intensity is 261 μmol $m^{-2}$ $s^{-1}$.

### A.3. The Trapezoidal rule

The Trapezoidal rule is shown in Eq. (A1). The 10-step approximation of Eq. (11b) is shown in Eq. (A2). Because both of the current PBRs have similar thickness of 0.025 m, the step length of the 10-step Trapezoidal rule is thereby calculated to be 0.0025 m.

$$\int_a^b f(x)dx = \frac{b-a}{2n} \cdot \sum_{i=1}^{n} (f(a) + 2f(x_i) + f(b)) \quad \text{(A1)}$$

where $x_i = a + \frac{b-a}{n} \cdot i$, $i \in [1, n]$ and n is total step number. Eq. (11b) is then re-written as Eq. (A2). The accuracy of this approximation method is later verified.

$$\bar{k}(I) = \frac{1}{20} \cdot \sum_{i=1}^{10} (k(I_0) + 2k(I_i) + k(I_{0.025})) \quad \text{(A2)}$$

Similarly, when simulating the influence of incident light intensity on hydrogen production rate, the average value of $h(I)$ is calculated by Eq. (A3).

$$\bar{h}(I) = \frac{1}{20} \cdot \sum_{i=1}^{10} (h(I_0) + 2h(I_i) + h(I_{0.025})) \quad \text{(A3)}$$

## References

[1] S. Aiba, Growth kinetics of photosynthetic microorganisms, Adv. Biochem. Eng. 23 (1982) 85–156.
[2] G. Alagappan, R.M. Cowan, Effect of temperature and dissolved oxygen on the growth kinetics of pseudomonas putida F1 growing on benzene and toluene, Chemosphere 54 (8) (2004) 1255–1265.
[3] S. Alagesan, et al., Model based optimization of high cell density cultivation of nitrogen-fixing cyanobacteria, Bioresour. Technol. 148 (2013) 228–233.
[4] U.K. Aryal, et al., Proteome analyses of strains ATCC 51142 and PCC 7822 of the diazotrophic cyanobacterium *Cyanothece* sp. under culture conditions resulting in enhanced hydrogen production, Appl. Environ. Microbiol. 79 (4) (2013) 1070–1077.
[5] A. Bandyopadhyay, et al., High rates of photobiological H2 production by a cyanobacterium under aerobic conditions, Nat. Commun. 1 (2010) 139 (Available at: http://www.ncbi.nlm.nih.gov/pubmed/21266989 [Accessed June 3, 2014]).
[6] Q. Béchet, A. Shilton, B. Guieysse, Modeling the effects of light and temperature on algae growth: state of the art and critical assessment for productivity prediction during outdoor cultivation, Biotechnol. Adv. 31 (8) (2013) 1648–1663 (Available at: http://www.ncbi.nlm.nih.gov/pubmed/23981914 [Accessed August 7, 2014]).
[7] V.S. Brauer, et al., Low temperature delays timing and enhances the cost of nitrogen fixation in the unicellular cyanobacterium Cyanothece, ISME J. 7 (11) (2013)

2105–2115 (Available at: http://www.ncbi.nlm.nih.gov/pubmed/23823493 [Accessed September 4, 2014]).
[8] L. Brennan, P. Owende, Biofuels from microalgae—a review of technologies for production, processing, and extractions of biofuels and co-products, Renew. Sust. Energ. Rev. 14 (2) (2010) 557–577 (Available at: http://linkinghub.elsevier.com/retrieve/pii/S1364032109002408 [Accessed July 9, 2014]).
[9] R. Chaubey, et al., A review on development of industrial processes and emerging techniques for production of hydrogen from renewable and sustainable sources, Renew. Sust. Energ. Rev. 23 (2013) 443–462 (Available at: http://linkinghub.elsevier.com/retrieve/pii/S1364032113001214 [Accessed July 12, 2014]).
[10] W. Chu, Biotechnological applications of microalgae, Int. E-J. Sci. Med. Educ. 6 (126) (2012) 24–37.
[11] Z. Cui, L.S. Fan, Turbulence energy distributions in bubbling gas–liquid and gas–liquid–solid flow systems, Chem. Eng. Sci. 59 (8–9) (2004) 1755–1766 (Available at: http://linkinghub.elsevier.com/retrieve/pii/S0009250904000909 [Accessed May 30, 2014]).
[12] P. Dechatiwongse, S. Srisamai, et al., Effects of light and temperature on the photoautotrophic growth and photoinhibition of nitrogen-fixing cyanobacterium *Cyanothece* sp. ATCC 51142, Algal Res. 5 (2014) 103–111 (Available at: http://linkinghub.elsevier.com/retrieve/pii/S2211926414000563 [Accessed July 14, 2014]).
[13] B. Patel, B. Tamburic, F.W. Zemichael, P. Dechatiwongse, K. Hellgardt, Algal biofuels: a credible prospective? ISRN Renewable Energy 2012: 63157 (2012) (Available at: http://www.hindawi.com/journals/isrn/2012/631574/).
[14] P. Dechatiwongse, D. Zhang, A. Del-Rio-Chanona, V. Vassiliadis, G. Maitland, K. Hellgardt, Effects of light intensity and temperature upon hydrogen production of nitrogen-fixing cyanobacterium Cyanothece sp. ATCC 51142. Algal1 Res. (2015) (provisional) (in preparation).
[15] P. Dechatiwongse, G.C. Maitland, K. Hellgardt, Demonstration of a two-stage aerobic / anaerobic chemostat for the enhanced production of hydrogen and biomass from unicellular nitrogen-fixing cyanobacterium. Algal Res. (2015) (submitted to the journal).
[16] D. Dutta, et al., Hydrogen production by Cyanobacteria, Microb. Cell Factories 4 (2005) 36 (Available at: http://www.pubmedcentral.nih.gov/articlerender.fcgi?artid=1343573&tool=pmcentrez&rendertype=abstract [Accessed July 23, 2014]).
[17] O. Elsharnouby, et al., A critical literature review on biohydrogen production by pure cultures, Int. J. Hydrog. Energy 38 (12) (2013) 4945–4966 (Available at: http://linkinghub.elsevier.com/retrieve/pii/S0360319913003984 [Accessed August 27, 2014]).
[18] S. Fouchard, et al., Kinetic modeling of light limitation and sulfur deprivation effects in the induction of hydrogen production with *Chlamydomonas reinhardtii*: Part I. Model development and parameter identification, Biotechnol. Bioeng. 102 (1) (2009) 232–245 (Available at: http://www.ncbi.nlm.nih.gov/pubmed/18688816).
[19] W.E. Hart, et al., Pyomo-optimization Modeling in Python, Springer, 2012.
[20] G. Kufryk, Advances in utilizing cyanobacteria for hydrogen production, Adv. Microbiol. 3 (6) (2013) 60–68.
[21] K. Kumar, C. Dasgupta, B. Nayak, Development of suitable photobioreactors for $CO_2$ sequestration addressing global warming using green algae and cyanobacteria, Bioresour. Technol. 102 (8) (2011) 4945–4953.
[22] T.M. Mata, MartinsA.a. , N.S. Caetano, Microalgae for biodiesel production and other applications: a review, Renew. Sust. Energ. Rev. 14 (1) (2010) 217–232 (Available at: http://linkinghub.elsevier.com/retrieve/pii/S1364032109001646 [Accessed July 9, 2014]).
[23] A. Melis, et al., Sustained photobiological hydrogen gas production upon reversible inactivation of oxygen evolution in the green alga *Chlamydomonas reinhardtii*, Plant Physiol. 122 (1) (2000) 127–136 (Available at: http://www.pubmedcentral.nih.gov/articlerender.fcgi?artid=58851&tool=pmcentrez&rendertype=abstract).
[24] H. Min, L.a. Sherman, Hydrogen production by the unicellular, diazotrophic cyanobacterium *Cyanothece* sp. strain ATCC 51142 under conditions of continuous light, Appl. Environ. Microbiol. 76 (13) (2010) 4293–4301 (Available at: http://www.pubmedcentral.nih.gov/articlerender.fcgi?artid=2897434&tool=pmcentrez&rendertype=abstract).
[25] M. Morbidelli, A. Varma, A generalized criterion for parametric sensitivity: application to thermal explosion theory, Chem. Eng. Sci. 43 (1) (1988) 91–102.
[26] B.-J. Ni, et al., Formation of distinct soluble microbial products by activated sludge: kinetic analysis and quantitative determination, Environ. Sci. Technol. 46 (3) (2012) 1667–1674 (Available at: http://www.ncbi.nlm.nih.gov/pubmed/22185635).
[27] I. Rawat, et al., Biodiesel from microalgae: a critical evaluation from laboratory to large scale production, Appl. Energy 103 (2013) 444–467 (Available at: http://linkinghub.elsevier.com/retrieve/pii/S0306261912007088 [Accessed July 11, 2014]).
[28] M. a Schneegurt, et al., Compositional and toxicological evaluation of the diazotrophic cyanobacterium, *Cyanothece* sp. strain ATCC 51142, Aquaculture (Amsterdam, Netherlands) 134 (1995) 339–349 (Available at: http://www.ncbi.nlm.nih.gov/pubmed/11539278).
[29] J.M.F. Sevilla, F.G.A. Fernandez, A.C. Gomez, A mathematical model of microalgal growth in light-limited chemostat culture, J. Chem. Technol. Biotechnol. 61 (1994) 167–173.
[30] E. Stephens, et al., Future prospects of microalgal biofuel production systems, Trends Plant Sci. 15 (10) (2010) 554–564 (Available at: http://www.ncbi.nlm.nih.gov/pubmed/20655798 [Accessed September 3, 2014]).
[31] E. Suli, D. Mayers, An Introduction to Numerical Analysis, Cambridge University Press, Cambridge, 2012.
[32] B. Tamburic, et al., Process and reactor design for biophotolytic hydrogen production, Phys. Chem. Chem. Phys 15 (26) (2013) 10783–10794 (Available at: http://www.ncbi.nlm.nih.gov/pubmed/23689756 [Accessed August 30, 2014]).
[33] J.V.C. Vargas, et al., The microalgae derived hydrogen process in compact photobioreactors, Int. J. Hydrog. Energy 39 (18) (2014) 9588–9598 (Available at: http://linkinghub.elsevier.com/retrieve/pii/S0360319914011495 [Accessed September 4, 2014]).
[34] I. Vatcheva, et al., Experiment selection for the discrimination of semi-quantitative models of dynamical systems, Artif. Intell. 170 (4–5) (2006) 472–506 (Available at: http://linkinghub.elsevier.com/retrieve/pii/S0004370205002092 [Accessed July 12, 2014]).
[35] A. Wächter, L.T. Biegler, On the Implementation of an Interior-point Filter Line-search Algorithm for Large-scale Nonlinear ProgrammingAvailable at: http://link.springer.com/10.1007/s10107-004-0559-y2005.
[36] D. Zhang, et al., Analysis of the cyanobacterial hydrogen photo-production process via model identification and process simulation, Chemical Engineering Science, 2015. (Available at: http://linkinghub.elsevier.com/retrieve/pii/S0009250915000883 [Accessed February 16, 2015]).
[37] D. Zhang, P. Dechatiwongse, K. Hellgardt, Modelling light transmission, cyanobacterial growth kinetics and fluid dynamics in a laboratory scale multiphase photo-bioreactor for biological hydrogen production, Algal Res. 8 (2015) 99–107 (Available at: http://www.sciencedirect.com/science/article/pii/S2211926415000181#).
[38] D. Zhang, N. Xiao, K.T. Mahbubani, E.A. del Rio-Chanona, N.K.H. Slater, V.S. Vassiliadis, Bioprocess modelling of biohydrogen production by Rhodopseudomonas palustris: model development and effects of operating conditions on hydrogen yield and glycerol conversion efficiency, Chem. Eng. Sci. 130 (2015) 68–78, http://dx.doi.org/10.1016/j.ces.2015.02.045.
[39] J. Cabello, M. Morales, S. Revah, Dynamic photosynthetic response of the microalga Scenedesmus obtusiusculus to light intensity perturbations. Chem. Eng. J. 252 (2014) 104–111 (Available at: http://linkinghub.elsevier.com/retrieve/pii/S1385894714005051).
[40] H.J. Gons, Dynamic modelling of viral impact on cyanobacterial populations in shallow lakes: implications of burst size, Mar. Biol. Assoc. U. K. 86 (2006) 537–542.
[41] R.W.F. Hardy, R.C. Burns, R.D. Holsten, Applications of the acetylene-ethylene assay for measurement of nitrogen fixation, Soil Biol. Biochem. 5 (1) (1973) 47–81.
[42] H. Topiwala, C.G. Sinclair, Temperature relationship in continuous culture, Biotechnol. Bioeng. XIII (1971) 795–813.